Optical functions of ion-implanted, laser-annealed heavily doped silicon

G. E. Jellison, Jr., S. P. Withrow, J. W. McCamy, J. D. Budai, D. Lubben, and M. J. Godbole
Solid State Division, Oak Ridge National Laboratory, Oak Ridge, Tennessee 37831-6030
(Received 6 July 1995)

The optical functions of silcon heavily doped with Ge, P, As, and B are determined using spectroscopic ellipsometry measurements from 240 to 840 nm (5.16 to 1.47 eV). Below the direct band gap, there is a residual enhancement of the optical-adsorption coefficient for silicon heavily doped with *n*-type dopants, which cannot be explained by surface roughness. In the low-energy region of the observed spectrum, it is found that both free-carrier and strain effects alter the complex dielectric function.

I. INTRODUCTION

The optical properties of very heavily doped silicon have been the subject of many investigations over the last three decades. Technologically, these studies are important because they serve to characterize a material often used in many semiconductor devices. In addition, these studies have aroused considerable scientific interest because they give insight into the electronic nature of the heavily doped material.

About 20 years ago, it was discovered that one way of forming very heavily doped silicon was by ion implantation followed by pulsed-laser annealing.[1] The material thus formed was a nearly perfect single crystal, with far fewer dislocation loops than normally found in furnace-annealed, ion-implanted silicon. Moreover, the ion-implantation, pulsed-laser annealing process was able to form metastable phases, whereby much higher concentrations of the implanted species could be incorporated into the lattice on substitutional sites than with traditional techniques. Later work showed that laser annealing was very useful for forming large area junctions in semiconductor devices, where it was used to fabricate solar cells with close to 20% efficiencies.[2]

For photon energies well below the indirect band gap of silicon (~ 1.16 eV or 1.07 μm), the optical spectra are dominated by free-carrier effects.[3–7] Near the indirect band edge, the optical absorption is modified because the Fermi level is pinned in either the conduction or valence band, resulting in an effective increase in the optical band gap.[8] Near and above the direct band edge (~ 3.4 eV or 370 nm in silicon), the optical effects are dominated by direct transitions.[9] In this region of the spectrum, the heavy doping broadens the critical points and shifts them to lower energies; usually, doping densities greater than $\sim 10^{19}$ atoms/cm^3 are required to see these effects.

In the photon energy region from 1.16 to 3.4 eV (1070 to 370 nm), optical absorption in silicon is dominated by indirect optical transitions, requiring a phonon to conserve lattice momentum. Aspnes *et al.*[10] and Jellison *et al.*[11] presented ellipsometric data for silicon heavily doped with As, which indicated that there was an enhancement in the optical absorption in this photon energy range due to the heavy doping. In Ref. 11, the effect was observed most markedly with As doping, and was not observed in P- or B-doped materials, although the P- and B-doped samples that were examined were not nearly as heavily doped as were the As-doped samples. Later, Aspnes, Studna, and Kinsbron[12] stated that this ellipsometric data could be explained by a surface roughness overlayer on the samples, and was not necessarily an intrinsic increase in optical absorption due to heavy doping effects.

In this paper, we present results of spectroscopic ellipsometry studies of heavily doped silicon fabricated using ion implantation followed by pulsed-laser annealing. We will show that there is indeed a heavy doping effect on the optical properties of silicon below the direct band edge which cannot be due to surface roughness. An enhanced optical absorption is observed in both P- and As-doped samples, which is much stronger than observed in B-doped samples; all samples show the optical effects of free carriers. The boron-doped samples also show the effects of strain-induced changes in the dielectric function. We also show the results of spectroscopic ellipsometry measurements of Ge-implanted samples; these measurements show that ion implantation followed by pulsed-laser annealing does not, by itself, appreciably change the optical properties of the near-surface region.

Although the ellipsometric data presented in this paper show clear evidence of critical point broadening and moving to lower energy with increasing doping, these critical points are not the subject of this paper. Interested readers are referred to Viña and Cardona.[9]

II. EXPERIMENT

Samples of heavily doped silicon were fabricated by ion implanting B, P, As, and Ge into silicon followed by pulsed-laser annealing. We used a single excimer laser pulse (XeCl, 70-ns pulse width, 308 nm, 1.7 J/cm^2) to anneal each of the samples. Previous samples[11] were annealed with ten shots from a ruby laser (694 nm); although this treatment gave a more abrupt dopant profile, it could also have resulted in more surface roughness. The single laser pulse minimizes any introduced surface roughness, but does result in a more diffuse dopant profile. Table I summarizes the samples used in this

0163-1829/95/52(20)/14607(8)/$06.00

TABLE I. The implantation dose and average carrier concentration for the samples examined in this study.

Name	Implant dose ($\times 10^{14}$/cm^2)	Average conc. (N) ($\times 10^{20}$/cm^3)
Si:Ge 3×10^{14}	3	0.23
Si:Ge 1×10^{15}	10	0.77
Si:Ge 3×10^{15}	30	2.3
Si:Ge 1×10^{16}	100	7.7
Si:P 3×10^{14}	3	0.23
Si:P 1×10^{15}	10	0.77
Si:P 3×10^{15}	30	2.3
Si:P 1×10^{16}	100	7.7
Si:P 3×10^{16}	300	23
Si:As 3×10^{14}	3	0.23
Si:As 1×10^{15}	10	0.77
Si:As 3×10^{15}	30	2.3
Si:As 1×10^{16}	100	7.7
Si:As 3×10^{16}	300	18
Si:B 5×10^{15}	50	3.8
Si:B 1×10^{16}	100	7.7
Si:B 1.5×10^{16}	150	11.5
Si:B 2×10^{16}	200	15.4
Si:B 3×10^{16}	300	23

study. When we refer to a specific sample, we will use the symbol of the dopant atom followed by the implantation dose in atoms/cm^2. Therefore, the silicon sample that was implanted with 3×10^{16} P atoms/cm^2 will be referred to as P 3×10^{16}.

Rutherford backscattering (RBS) measurements were used to characterize some of the heavier doped P-, As-, and Ge-implanted samples. This technique measures the dopant profile, the total number and identity of the dopant atoms, and whether or not the dopant atoms are substitutional. The dopant profile for As 3×10^{16} is shown in Fig. 1; all other measured profiles are scaled to that shown in Fig. 1, indicating that the pulsed-laser annealing determined the dopant profile, not the implantation conditions. A detailed analysis of dopant profiles after pulsed-laser annealing is given by Wood, Kirkpactrick, and Giles,[13] who also include references to the earlier experimental data. As can be seen, there is a rather long tail on the dopant profile extending beyond ~200 nm. All dopant atoms were substitutional, and all samples except the As 3×10^{16} sample incorporated all the implanted atoms. For the As 3×10^{16} sample, a total of 2.35×10^{16} As atoms/cm^2 were detected, indicating some loss of As for this sample during laser annealing. The average dopant concentration, denoted by N, was determined by dividing the surface implant dose by the thickness of the layer (110 nm; see Fig. 1); it is given in Table I.

It has already been shown that ion implantation of Si with B atoms, followed by pulsed ruby laser annealing ($\lambda=694$ nm), results in a significant strain of the near-surface region due to the smaller size of the B atom compared to Si.[14] At very high doping densities, this strain is relieved by cracking of the near-surface region.[15] Therefore, the B 3×10^{16} sample was also examined by x-ray

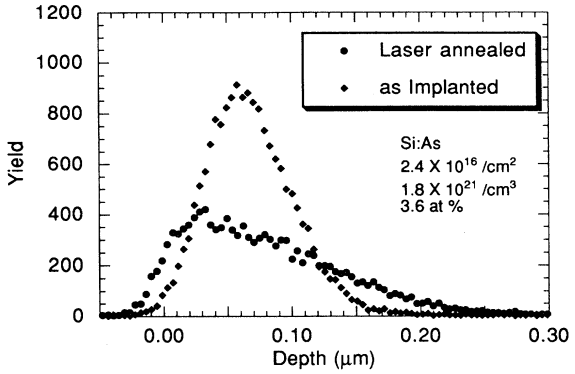

FIG. 1. Dopant profile for Si:As 3×10^{16}. The thickness of the layer is taken to be the full width at half maximum (110 nm).

diffraction to measure the strain of the near-surface region, and by scanning electron microscopy to observe any possible microcracks. It was found that this sample experienced a relatively uniform 1.1% axially compressive strain, and no microcracking was observed.

Ellipsometric measurements were made with the two-channel spectroscopic polarization modulation ellipsometer (2C-SPME) (Ref. 16) from 1.48 to 5.16 eV (240 to 840 nm). The 2C-SPME measures the associated ellipsometric parameters, which are given by

$$N=\cos(2\psi)\ , \tag{1a}$$

$$S=\sin(2\psi)\sin(\Delta)\ , \tag{1b}$$

$$C=\sin(2\psi)\cos(\Delta)\ . \tag{1c}$$

The associated ellipsometry parameters are related to the standard ellipsometry parameters, which are defined by[17]

$$r_p/r_s=\rho=\tan\psi e^{i\Delta}\ , \tag{2}$$

where the quantities r_p and r_s are the Fresnel reflection coefficients for light polarized parallel and perpendicular to the plane of incidence.

The complex dielectric function $\varepsilon(\lambda)$ of a material (or equivalently, its complex refractive index), is given by

$$\varepsilon=\varepsilon_1+i\varepsilon_2=\tilde{n}^2=(n+ik)^2\ , \tag{3}$$

where ε_1 and ε_2 are the real and imaginary parts of ε, and n and k are the refractive index and extinction coefficient, respectively. A common way of expressing ellipsometric data is the pseudodielectric function, given by

$$\langle\varepsilon\rangle=\varepsilon_a\sin^2\phi\left[1+\tan^2\phi\left[\frac{(1-\rho)}{(1+\rho)}\right]^2\right]\ , \tag{4}$$

where ϕ is the angle of incidence and ε_a is the dielectric function of the ambient. If the sample being studied can be modeled using the simple two-phase model, then the pseudodielectric function is equal to the dielectric function of the material. Another parameter of interest is the optical-absorption coefficient, which is given by

$$\alpha=4\pi k/\lambda\ , \tag{5}$$

where λ is the wavelength of light.

For the case of silicon well below the direct band edge (where α and k are relatively small) and with a small overlayer such as a native oxide, the ellipsometric angle ψ and Δ can be linearized using the following relations:

$$\psi = g_1 n + g_2 \phi \ , \tag{6a}$$

$$\Delta = h_1 k + h_2 d \ , \tag{6b}$$

where n and k are the refractive index and extinction coefficient of the substrate, ϕ is the angle of incidence, and d is the product of the thickness and refractive index of the overlayer; the quantities g_1, g_2, h_1, and h_2 are scaling constants. Therefore, if one is to measure n and k accurately, one has to measure ψ and Δ very accurately, and ϕ and d must be separately determined.

Many of the previous ellipsometric measurements of heavily doped silicon in the literature (including Refs. 9, 10, and 11) have been performed using a rotating analyzer ellipsometer (RAE). The RAE instruments measure functions of N and C, but cannot measure S. For measurements near and above the direct band edge, the measurement of S is not important; however, below the direct band edge, k can become very small, resulting in Δ being near 0° or 180°, so the measurement of the S parameter becomes imperative. The measurements to be discussed in this paper have been performed using the 2C-SPME (see Ref. 16 for more details), where S can be measured very accurately.

For some samples, additional measurements were taken using a nulling ellipsometer at 1152 nm ($\sim$1.076 eV). This wavelength is below the indirect band edge of undoped silicon, where the absorption coefficient from intrinsic silicon is close to 0. (Note that α will be greater than 0 for the heavily doped samples due to free-carrier effects.) To check for consistency, these measurements were performed at two different angles of incidence (69.06° and 64.44°).

III. DATA ANALYSIS

In order to determine the dielectric functions of heavily doped silicon from the ellipsometric data, one must first start with a model of the sample surface. In this case, a realistic model would consist of air, surface overlayer (native oxide and/or surface roughness), heavily doped silicon, and undoped silicon. Given that the dopant profile (shown in Fig. 1) is far from abrupt, one might have to invoke a more complicated model of the heavily doped region, consisting of several layers. The proposed model is then used to calculate the Fresnel reflection coefficients and the quantity ρ is calculated [see Eq. (2)].

However, if the change in the refractive index with thickness is small, then the light will be minimally reflected from the refractive index gradient. This type of profile is often treated with an analog of the WKB approximation,[18] which means that the profile change is ignored, taking the surface refractive index as the refractive index of the entire layer. In this case, the surface model is simplified to air/surface overlayer/heavily doped silicon. In order for the WKB approximation to be used for a layer,

$$\frac{1}{\beta}\frac{d^2\beta}{d\theta^2} \ , \quad \frac{1}{\beta}\frac{d\beta}{d\theta} \ll 1 \ , \tag{7a}$$

where

$$\beta = \cos\phi / \tilde{n}(0) \quad (r_p \text{ or TM}) \tag{7b}$$

$$= \tilde{n}(0)\cos\phi \quad (r_s \text{ or TE}) \ , \tag{7c}$$

$$\theta(d) = \frac{2\pi}{\lambda}\int_0^d \tilde{n}(x)\cos\phi(x)dx \quad (0 \text{ to } d) \ . \tag{7d}$$

In Eqs. (7), the integration is performed over film thickness 0 to d, where d is the nominal thickness of the heavily doped region, ϕ is the angle of incidence in the medium, and $\theta(d)$ is the optical thickness at thickness d. These criteria are satisfied whenever the index gradient is small with respect to the wavelength of light. For example, if the dielectric function varies linearly with respect to thickness, then, for a layer of thickness d, these criteria reduce to

$$\frac{\left[\lambda\frac{\partial\varepsilon}{\partial x}\right]^2}{\varepsilon^3 4\pi^2} = \frac{(\varepsilon_{\text{top}}-\varepsilon_{\text{bottom}})^2}{(\varepsilon_{\text{ave}})^3}\left[\frac{\lambda}{2\pi d}\right]^2 \ll 1 \ , \tag{8}$$

where $\partial\varepsilon/\partial x$ is the derivative of the complex dielectric function as a function of thickness, and ε_{ave} is the average dielectric function of the layer. Clearly, the simple surface model is valid for lightly doped samples, since $(\varepsilon_{\text{top}}-\varepsilon_{\text{bottom}})$ (Ref. 2) is small. In the more heavily doped samples, the absorption coefficient is large (see below); however, the simplified model is also valid in this case, since the probability of light penetrating the layer, being reflected and then reemerging, is small. In some of the intermediately doped samples, this approximation breaks down for very small values of α. In all cases, the signature of the breakdown of the WKB approximation is the observation of oscillations in the ε_2, α, and k parameters calculated from the experimental data.

The 2C-SPME data were reduced to $\varepsilon_1, \varepsilon_2$ data using the simple air/overlayer/substrate model, assuming that the overlayer was 1.8-nm SiO_2. To calibrate the oxide thickness, the lightest doped samples of each ion implanted species was used as a standard. Using the 2C-SPME data in the 600–750-nm range, an oxide thickness of 1.8 ± 0.2 nm was found; this oxide layer thickness was used for all samples.

IV. RESULTS AND DISCUSSION

Before the data are presented, it is instructive to present the pseudodielectric functions that one would obtain from a silicon substrate with varying thickness of surface roughness, shown in Fig. 2. Recall that the pseudodielectric function is equal to the actual dielectric function only when no overlayer is present; therefore, this figure shows the error resulting from overlayers that are not taken into account. These calculations were performed assuming that the surface overlayer consisted of 50% Si, 50% voids, calculated using the Bruggeman effective-medium approximation;[19] the dielectric func-

tions for crystalline silicon were taken from Ref. 20. As can be seen from this figure, even a 1-nm surface roughness layer alters the pseudodielectric functions significantly. As has been discussed by Aspnes, Studna, and Kinsbron,[12] surface roughness increases $\langle \varepsilon_2 \rangle$ below the direct band edge, and decreases $\langle \varepsilon_2 \rangle$ for all energies above the direct band edge.

Figure 3 shows the resulting dielectric functions obtained from silicon that had been implanted with 1×10^{16} Ge atoms/cm^2, followed by pulsed-laser annealing. As can be seen from the figure, the dielectric functions of the ion-implanted, pulse-laser-annealed samples are nearly the same as the unimplanted, unannealed silicon sample. In particular, there is no effect on the optical-absorption coefficient at low photon energies (not shown). These results strongly indicate that the process of ion implantation followed by pulsed-laser annealing by itself does very little to alter the optical properties of the near-surface region.

For the *n*-type dopants P and As, shown in Figs. 4 and 5, respectively, there is indeed a strong dopant effect.

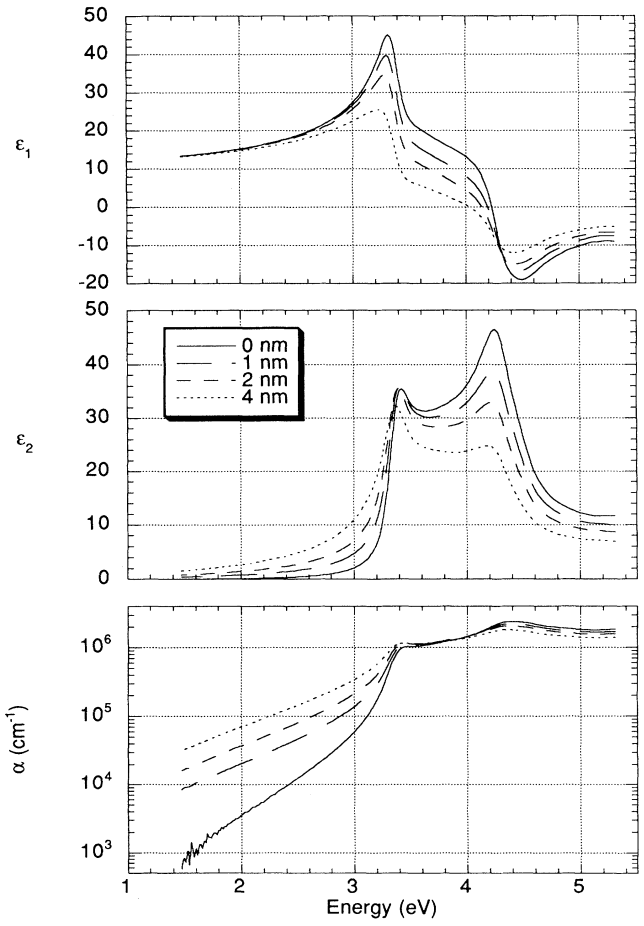

FIG. 2. Pseudodielectric functions and pseudoabsorption coefficient of silicon calculated by assuming a 50% void, 50% silicon effective-medium overlayer; four different overlayer thicknesses were calculated, as noted on the figure. These are the spectra one would obtain if the sample surface were perturbed by an unknown roughness layer.

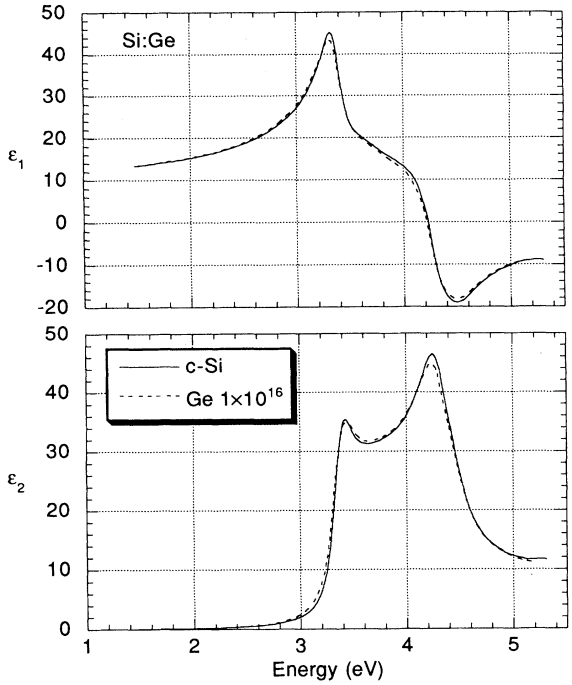

FIG. 3. Dielectric functions of Si:Si implanted with 10^{16} Ge atoms/cm^2 ($\sim7.7\times10^{20}$ Ge/cm^3) and pulsed-laser annealed. The data for undoped silicon (*c*-Si) are taken from Ref. 30.

Below the direct band edge, there is a significant increase in the optical-absorption coefficient. The critical points (at 3.4 and 4.25 eV) are broadened and decrease in energy (discussed in detail in Ref. 9). However, note that there is very little change in the dielectric functions near 5 eV. Therefore, it is unlikely that surface roughness could be responsible for the increase in α below the direct band edge, but not affect either ε_1 or ε_2 near 5 eV (see Fig. 2). A very small oscillation in $\log_{10}(\alpha)$ is observable in the low-energy end of the 1×10^{16} samples, indicating a small breakdown of the WKB approximation (the oscillation amplitude in α is only about a factor of 1.5–2 times the error in α at these energies).

Similar results for boron-doped silicon are shown in Fig. 6. As with the *n*-type dopants, the critical points in the optical spectrum are significantly altered by the heavy doping. However, there is little if any increase in the optical-absorption coefficient below the direct band edge (within the error of the experiment). Note that the heavily doped samples show an oscillation in α below 2 eV, indicating a small breakdown in the WKB approximation. The oscillation amplitude is small ($\lesssim 2$–4 times the error in α) but larger than observed for the *n*-type samples.

A. Free-carrier effects

One possible perturbation of the dielectric functions of heavily doped semiconductors comes from free-carrier effects. For free electrons in a solid, the Drude theory states that the normal dielectric functions are perturbed using the following expression:

$$\varepsilon(\omega)=\varepsilon_0(\omega)-\frac{4\pi N}{m^*}\frac{e^2}{m_0}\left[\frac{\tau^2-i\tau/\omega}{1+\omega^2\tau^2}\right]. \quad (9)$$

In Eq. (9), N is the carrier concentration; m^* is the ratio of the effective mass to the mass of the electron; m_0; e is the electronic charge; τ is the free-carrier relaxation time; and ω is the angular frequency of the photon ($\omega=2\pi c/\lambda$, where c is the speed of light). The quantity $\varepsilon_0(\omega)$ is the dielectric function of undoped silicon. If $\omega^2\tau^2\gg1$, then Eq. (9) can be simplified to

$$\varepsilon(\omega)=\varepsilon_0(\omega)-\frac{4\pi N}{m^*}\frac{e^2}{m_0}\left[\frac{1-i/\omega\tau}{\omega^2}\right] \quad (10a)$$

or

$$\varepsilon(\lambda)=\varepsilon_0(\lambda)-\frac{4\pi N}{m^*}\frac{e^2}{m_0}\lambda^2\left[\frac{1-i\lambda/(2\pi c\tau)}{(2\pi c)^2}\right]. \quad (10b)$$

Equations (10) show that a linear plot of $\varepsilon_1(\lambda)-\varepsilon_{10}(\lambda)$ (the real part of the dielectric function) versus λ^2 should produce a straight line with slope $(4\pi N/\rho^*)(e^2/m_0)/(2\pi c)^2$. Figure 7 (bottom) shows three such plots for Si:As. As can be seen, $\varepsilon_1(\lambda)-\varepsilon_{10}(\lambda)$ is linear with nearly a zero intercept (within error limits) for all samples. For the case of the As 3×10^{16} fit, the reduced $\chi^2=0.16$, and the regression coefficient is 0.997, both indicating a good fit. From the slope and its error, N/m^* is determined to be $6.2\pm0.3\times10^{21}/\text{cm}^3$. The factor N/m^* can also be obtained from the nulling ellipsometry results at 1152 nm, and was found to be $5.7\pm0.3\times10^{21}/\text{cm}^3$. The B-doped samples (Fig. 7, top) showed the same linear behavior of $\varepsilon_1(\lambda)-\varepsilon_{10}(\lambda)$, except that the zero-wavelength intercept was negative (discussed below).

If N is taken to be the peak dopant concentration, then one can calculate the effective-mass ratio m^*, shown in Fig. 8. For the case of p-type silicon, the effective masses at lower doping densities agree with the older values obtained from cyclotron resonance studies (see Refs. 3 and

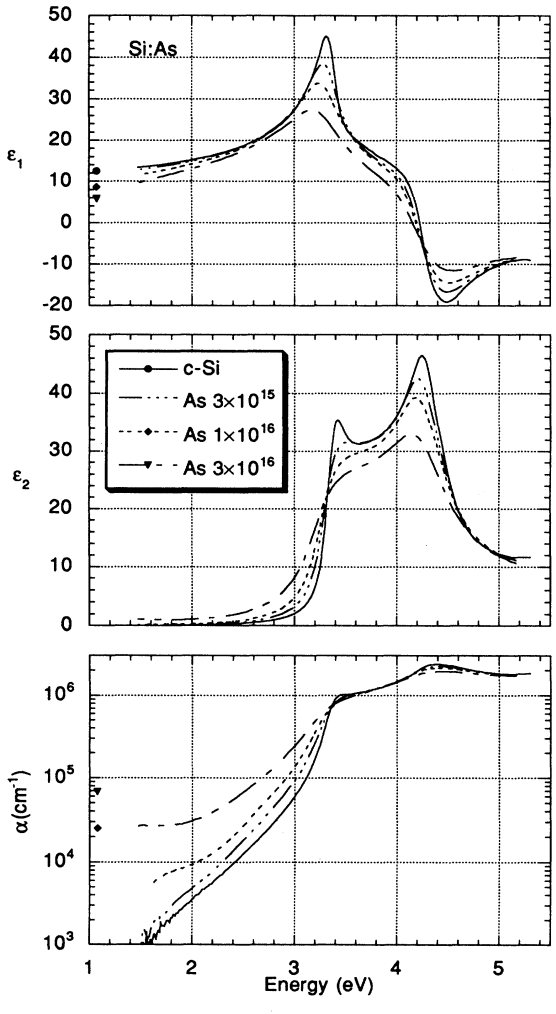

FIG. 4. Dielectric functions and optical-absorption coefficient of Si:As after pulsed-laser annealing shown for several different implantation doses of As. The data for undoped silicon (c-Si) are taken from Ref. 20.

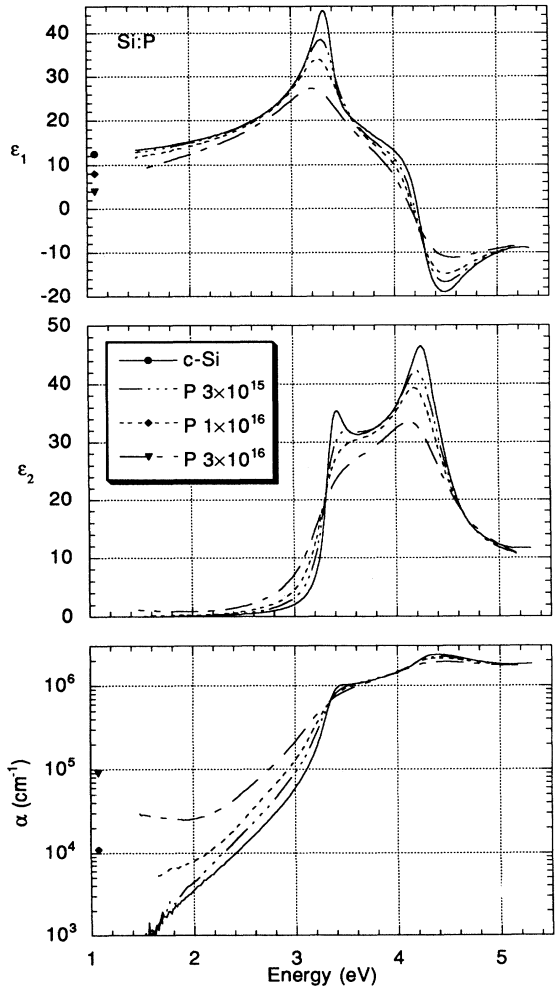

FIG. 5. Dielectric functions and optical-absorption coefficient of Si:P after pulsed-laser annealing shown for several different implantation doses of P. The data for undoped silicon (c-Si) are taken from Ref. 20.

4) (*NB*. If the split-off band is included in the calculation then $m^*=0.36$; see Refs. 5.) At the highest doping density, m^* is larger than the nominal value, indicating a breakdown in the parabolic band approximation inherent in the calculation[4] of m^*. For n-type materials, m^* is slightly lower than the nominal value at lower doping densities, and increases with increasing doping densities. It has been suggested by Miyao *et al.*[7] that this is due to the filling of another conduction band at higher doping densities.

Equations (9) and (10) show that the imaginary part of the dielectric function is also affected by free-carrier effects, but the free-carrier relaxation time becomes important. The nulling ellipsometry results at 1152 nm were used to obtain the change in the imaginary part of the dielectric function at that wavelength. Using these data in Eq. (10), we obtained $\tau=1.8\pm0.3\times10^{-15}$ s for the three samples As 1×10^{16}, As 3×10^{16}, and P 3×10^{16} (the error in the P 1×10^{16} nulling ellipsometry data precluded a determination of τ). Because of the oscillations in α for the boron-doped samples, no meaningful measurements of $\delta\varepsilon_2$ were possible at 1152 nm. However, Engstrom[6] has determined $\tau\sim7\times10^{-15}$ s for similar samples using infrared reflectivity and transmission; we use this value for p-type samples.

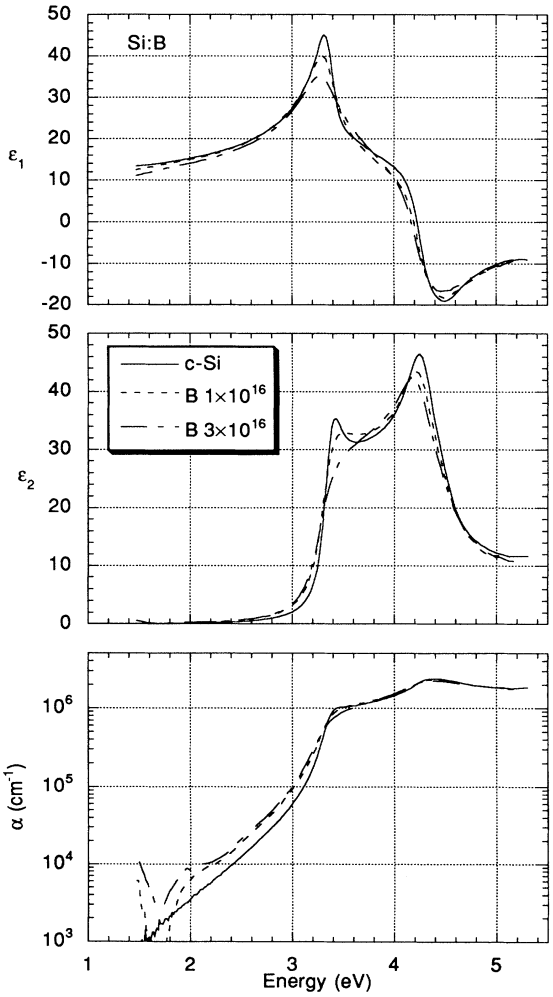

FIG. 6. Dielectric functions and optical-absorption coefficient of Si:B shown for several different implantation doses of B after pulsed-laser annealing. The data for undoped silicon (*c*-Si) are taken from Ref. 20.

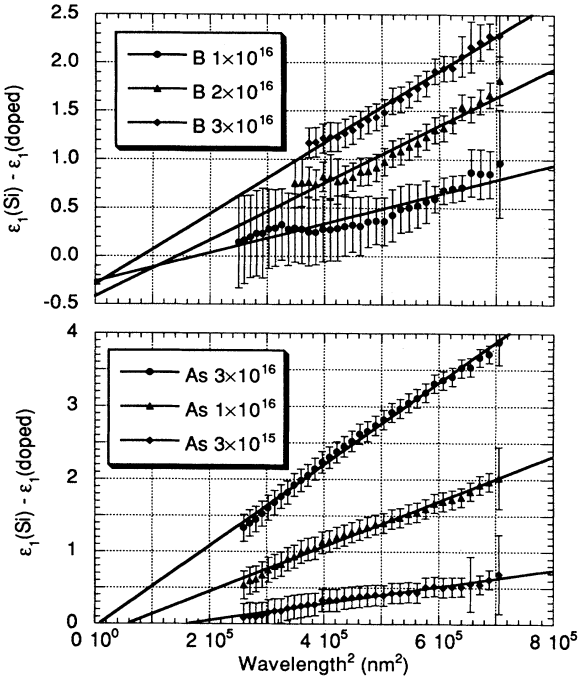

FIG. 7. The difference in the real part of the dielectric function between undoped silicon and heavily doped silicon at long wavelengths plotted vs the square of the wavelength. The results from boron-doped samples are shown at the top, and from As-doped samples at the bottom.

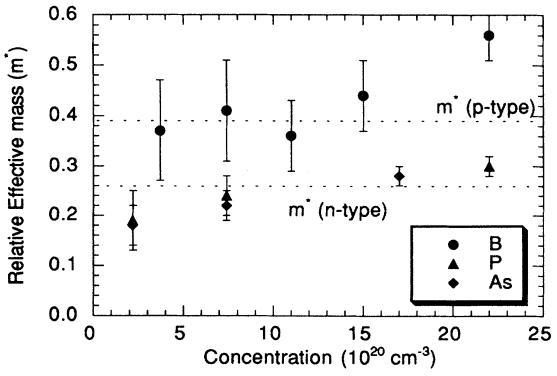

FIG. 8. The effective masses for n- and p-type heavily doped silicon vs the dopant density. The dotted lines indicate the effective masses calculated from effective masses determined from cyclotron resonance studies (see Ref. 4).

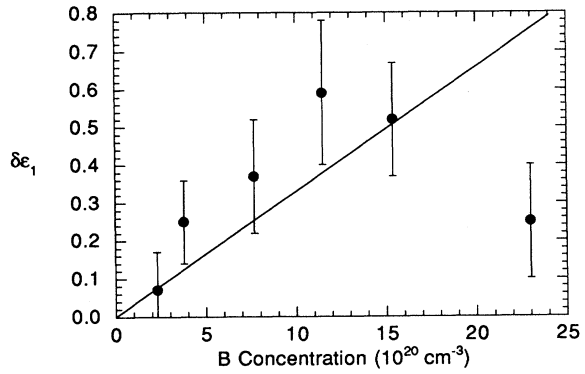

FIG. 9. The measured negative zero-wavelength intercept for heavily B-doped silicon, indicating a strain-induced change in the dielectric function. The straight line is a plot of Eq. (11d).

B. Strain-induced changes in the dielectric function

The boron atom is considerably smaller than the silicon atom. Therefore, large doses of boron ions implanted into silicon followed by laser annealing result in the near-surface region being compressively strained.[14] Optically, the near-surface region of the sample is uniaxial with the optic axis perpendicular to the surface of the sample. For a sample with such a strain pattern, the birefringence will be given by

$$\Delta\varepsilon=\varepsilon_{\text{para}}-\varepsilon_{\text{perp}}=e_{zz}(P_{11}-P_{12})(C_{11}-C_{12})\ , \qquad (11a)$$

and the bulk change in the dielectric function will be given by

$$\delta\varepsilon=\frac{(\varepsilon_{\text{para}}+2\varepsilon_{\text{perp}})}{3}-\varepsilon_0$$

$$=\frac{e_{zz}}{3}(P_{11}+2P_{12})(C_{11}+2C_{12})\ . \qquad (11b)$$

In Eqs. (11), e_{zz} is the strain, C_{11} and C_{12} are the stiffness of silicon ($C_{11}=166$ GPa and $C_{12}=64$ GPa), and P_{11} and

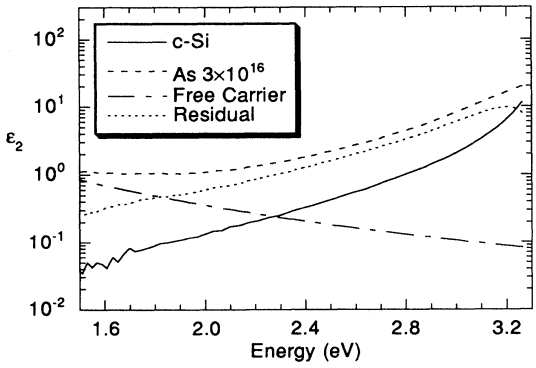

FIG. 10. The three contributions to ε_2 for the As 3×10^{16} sample. The values for *c*-Si are taken from Ref. 20, the free-carrier effects from Eqs. (10). The remaining part of ε_2 is shown as the residual ε_2 and is due to heavy doping effects.

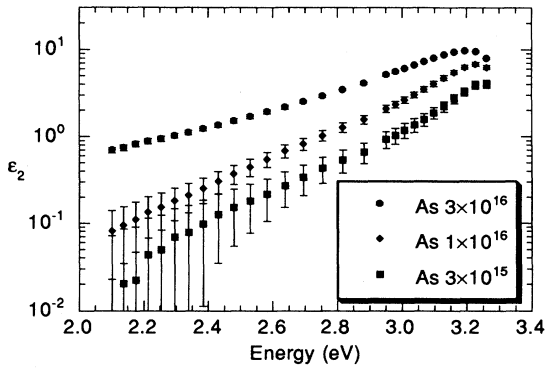

FIG. 11. The residual ε_2 for three As-doped silicon samples due to heavy doping effects.

P_{12} are the strain-optic coefficients (in the energy range 1–2 eV, $P_{11}-P_{12}=0.18$/GPa and $P_{11}+2P_{12}=0.7$/GPa from Ref. 21). Larson and co-workers measured $e_{zz}=-0.0055$ for an implantation dose of 1.0×10^{16} B/cm^2 and $e_{zz}=-0.0132$ for an implantation dose of 2.5×10^{16} B/cm^2, while we have measured $e_{zz}=-0.011$ for an implantation dose of 3.0×10^{16} B/cm^2. Given that slightly different dopant profiles can result from the different lasers used in annealing (ruby for the Larson work, excimer for this work), the results are in agreement. Using the measured strains of this work, we can relate the strain-induced changes in the dielectric function to boron concentration N_B, by

$$\Delta\varepsilon=-8.8\times10^{-23}N_B \quad \text{(birefringence)} \qquad (11c)$$

and

$$\delta\varepsilon=3.3\times10^{-22}N_B \quad \text{(bulk change)}\ . \qquad (11d)$$

As was mentioned above, the plot of ε_1 (Si) $-\varepsilon_1$ (B doped) (Fig. 7, top) shows a negative intercept, which is plotted versus boron concentration in Fig. 9. Up to $N_B\sim1.5\times10^{21}$/cm^3, $\delta\varepsilon$ is nearly linear with N_B, and fits Eq. (11d), shown as the straight line in Fig. 9; thus the offset can be explained by strain-induced changes in the real part of the dielectric function. For the most heavily doped sample, the measured value of $\delta\varepsilon_1$ is considerably below the value obtained from Eq. (11d), indicating an additional mechanism altering the dielectric function. Recall that the near-surface region of this sample consists of ~4% B atoms, and is therefore properly considered as a dilute alloy and not doped silicon.

C. Residual optical absorption

The imaginary part of the dielectric function consists of four parts: (1) a silicon part, given by the measured[20] ε_2; (2) a free-carrier part, given by Eqs. (9); (3) a strain part (for B dopants), given by Eq. (11d); and (4) a residual part, which includes the heavy doping effects. The free-carrier part of ε_2 is calculated using Eqs. (10), where

$(4\pi N/m^*)(e^2/m_0)$ is determined from Fig. 7 and $\tau \sim 1.8\times10^{-15}$ s. Figure 10 shows a partition of ε_2 for As 3×10^{16} into these three parts for photon energies between 1.5 and 3.2 eV. (Note: the results for the P 3×10^{16} sample are very similar, and it would be redundant to show the results.) In this energy region, the residual part is the dominant part, increasing the ε_2 by nearly a factor of 5 over the value of pure silicon. Similar plots of the residual part are shown in Fig. 11 for As 3×10^{16}, As 1×10^{16}, and As 3×10^{15}, which also show that the heavy doping significantly enhances the optical absorption in this energy region.

For B-doped samples, the effect is significantly less than for the *n*-type samples. Because of the larger effective mass and relaxation time, ε_2 from free-carrier effects is significantly smaller ($\sim$10–15% of that from *n*-type samples); in addition, the contribution due to residual absorption, which may be present, is at least 5–6 times less than that from *n*-type samples.

Therefore, the conclusion of Jellison *et al.*[11] that there is an enhancement of the optical absorption below the direct band gap for heavily As-doped silicon is essentially correct, but, contrary to Ref. 11, this enhancement also occurs for heavily P-doped samples as well. The enhancement cannot be due to surface roughness effects, as claimed by Aspnes, Studna, and Kinsbron.[12]

V. CONCLUSIONS

Using spectroscopic ellipsometry, we have examined several samples implanted with different concentrations of Ge, P, As, and B into silicon, followed by pulsed-laser annealing. Several conclusions can be made.

(1) The process of ion implantation followed by excimer pulsed-laser annealing does not appreciably affect the optical properties of the near-surface region by itself. This is indicated by the closeness of the dielectric functions of Ge-implanted Si compared to those for undoped Si.

(2) Free-carrier effects can be seen in both *n*- and *p*-type heavily doped silicon, but are larger for *n*-type silicon. The effective masses for both electrons and holes can be determined from the measurements, and agree reasonably well with other measurements.

(3) Strain in heavily boron-doped silicon has been observed using x-ray analysis. This strain leads directly to a predictable change in the dielectric function, with the exception of the heaviest doped sample.

(4) There is indeed a residual optical absorption due to heavy doping effects. This effect is much larger for *n*-type dopants than it is for *p*-type dopants, and does not depend upon the dopant species (As vs P).

[1] *Pulsed Laser Processing of Semiconductors,* edited by R. F. Wood, C. W. White, and R. T. Young, Semiconductors and Semimetals Vol. 23 (Academic, New York, 1984).

[2] R. F. Wood, R. D. Westbrook, and G. E. Jellison, Jr., Electron Device Lett. **EDL-8**, 249 (1987).

[3] H. Y. Fan, W. Spitzer, and R. J. Collins, Phys. Rev. **101**, 566 (1956).

[4] W. G. Spitzer and H. Y. Fan, Phys. Rev. **106**, 882 (1957).

[5] E. Barta, Infrared Phys. **17**, 111 (1977); **17**, 319 (1977); E. Barta and G. Lux, J. Phys. D **16**, 1543 (1983).

[6] H. Engstrom, J. Appl. Phys. **51**, 5245 (1980).

[7] M. Miyao, T. Motooka, N. Natsuaki, and T. Tokuyama, in *Laser and Electron-Beam Solid Interactions and Materials Processing,* edited by J. F. Gibbons, L. D. Hess, and T. W. Sigmon (Elsevier/North-Holland, Amsterdam, 1980), p. 163.

[8] J. I. Pankove, *Optical Processes in Semiconductors* (Dover, New York, 1971).

[9] L. Viña and M. Cardona, Phys. Rev. B **29**, 6739 (1984).

[10] D. E. Aspnes, G. K. Celler, J. M. Poate, G. A. Rozgonyi, and T. T. Sheng, in *Laser and Electron Beam Processing of Electronic Materials,* edited by C. L. Anderson, G. K. Celler, and G. A. Rozgonyi (Electrochemical Society, Princeton, 1980), Vol. 80-1, p. 414.

[11] G. E. Jellison, Jr., F. A. Modine, C. W. White, R. F. Wood, and R. T. Young, Phys. Rev. Lett. **46**, 1414 (1981).

[12] D. E. Aspnes, A. A. Studna, and E. Kinsbron, Phys. Rev. B **29**, 768 (1984).

[13] R. F. Wood, J. R. Kirkpatrick, and G. E. Giles, Phys. Rev. B **23**, 5555 (1981).

[14] B. C. Larson, C. W. White, and B. R. Appleton, Appl. Phys. Lett. **32**, 801 (1978); B. C. Larson and J. F. Barhorst, J. Appl. Phys. **51**, 3181 (1980).

[15] C. W. White, B. R. Appleton, B. Stritzker, D. M. Zehner, and S. R. Wilson, in *Laser and Electron-Beam Interactions and Materials Processing,* edited by J. F. Gibbons, L. D. Hess, and T. W. Sigmon, MRS Symposia Proceeding No. 1 (Materials Research Society, Pittsburgh, 1981), p. 59.

[16] G. E. Jellison, Jr. and F. A. Modine, Appl. Opt. **29**, 959 (1990).

[17] R. M. A. Azzam and N. M. Bashara, *Ellipsometry and Polarized Light* (North-Holland, Amsterdam, 1977).

[18] R. Jacobsson, in *Progress in Optics,* edited by E. Wolf (Wiley, New York, 1965), Vol. V, p. 247.

[19] D. A. G. Bruggeman, Ann. Phys. (Leipzig) **24**, 636 (1935).

[20] G. E. Jellison, Jr., Opt. Mater. **1**, 41 (1992).

[21] P. Etchegoin, J. Kircher, and M. Cardona, Phys. Rev. B **47**, 10 292 (1993).